



Cite this: *Chem. Commun.*, 2021, **57**, 2947

Received 14th January 2021,  
Accepted 17th February 2021

DOI: 10.1039/d1cc00250c

rsc.li/chemcomm

## A bioinspired oxoiron(IV) motif supported on a N<sub>2</sub>S<sub>2</sub> macrocyclic ligand†

Jennifer Deutscher,<sup>a</sup> Philipp Gerschel,<sup>b</sup> Katrin Warm,<sup>a</sup> Uwe Kuhlmann,<sup>c</sup> Stefan Mebs,<sup>d</sup> Michael Haumann,<sup>d</sup> Holger Dau,<sup>d</sup> Peter Hildebrandt,<sup>d</sup> Ulf-Peter Apfel<sup>d,\*be</sup> and Kallol Ray<sup>id,\*,a</sup>

**A mononuclear oxoiron(IV) complex 1-trans bearing two equatorial sulfur ligations is synthesized and characterized as an active-site model of the elusive sulfur-ligated Fe<sup>IV</sup>=O intermediates in non-heme iron oxygenases. The introduction of sulfur ligands weakens the Fe=O bond and enhances the oxidative reactivity of the Fe<sup>IV</sup>=O unit with a diminished deuterium kinetic isotope effect, thereby providing a compelling rationale for nature's use of the cis-thiolate ligated oxoiron(IV) motif in key metabolic transformations.**

Sulfur-ligated oxoiron(IV) centers are proposed as key oxidants in the catalytic cycles of various heme and non-heme iron oxygenases (Scheme 1).<sup>1–3</sup> Iron(IV)-oxo porphyrin  $\pi$ -cation radical (Cpd I) intermediates containing a thiolate ligand *trans* to the oxo group have been isolated and spectroscopically characterized in a number of heme enzymes.<sup>4–6</sup> The increased basicity of the oxoiron(IV) core caused by the strong electron donation from the *trans*-sulfur ligand, is discussed as a strategy to perform hydrogen atom abstraction by Cpd I at a lower redox potential without performing oxidative destruction of the surrounding enzyme environment.<sup>5,7–10</sup> However, similar knowledge on the effect of *cis*-sulfur ligands on the reactivity of oxoiron(IV) cores in non-heme enzymes is lacking. Notably, identification of *cis* thiolate-ligated oxoiron(IV) species remained elusive in biology, although they are suggested to be reactive intermediates for a wide range of chemical transformations, including sulfur-oxygenation,

hydrogen-atom abstraction, and C–S bond formation reactions in non-heme enzymes.

For over 40 years, small-molecule complexes synthesized as active-site models of the high-valent intermediates in heme and non-heme oxygenases have advanced our understanding of the catalytic cycles.<sup>3,11–20</sup> Despite these efforts, the synthesis of an oxoiron(IV) porphyrin complex with a thiolate ligand has not yet been achieved. Furthermore, [(TMCS)Fe<sup>IV</sup>(O)]<sup>+</sup> (TMCS = 1-mercaptoethyl-4,8,11-trimethyl-1,4,8,11-tetraazacyclotetra-decane; (Scheme 1)), represents the only synthetic complex<sup>21</sup> thus far to model the RS-Fe<sup>IV</sup>=O unit associated with the active oxidants of cytochrome P450<sup>2,6</sup> and chloroperoxidase.<sup>4,5,10</sup> Similarly, a recently reported [(Me<sub>3</sub>TACN)Fe<sup>IV</sup>(O)(S<sub>2</sub>Si(CH<sub>3</sub>)<sub>2</sub>)] (Me<sub>3</sub>TACN = 1,4,7-trimethyl-1,4,7-triazacyclononane)<sup>13</sup> complex represents the only model complex for the postulated oxoiron(IV) core containing a sulfur ligation *cis* to the oxo group in non-heme oxygenases.<sup>22,23</sup> However, the thermal instability of the compound has prevented any reactivity studies. Herein we report the synthesis and characterization of the *S* = 1 Fe<sup>IV</sup>=O complex [(dithiacyclam)Fe<sup>IV</sup>(O)(CH<sub>3</sub>CN)]<sup>2+</sup> (**1-trans**, dithiacyclam<sup>24,25</sup> = 1,8-dithia-4,11-diazacyclotetra-decane), which contains two thioether sulfur coordination sites poised *cis* to the oxo group. A comparative study between **1-trans**,



**Scheme 1** Top: Proposed structures of the thiolate-ligated oxoiron(IV) reactive intermediates in biology; bottom: structures of [(TMCS)Fe<sup>IV</sup>(O)]<sup>+</sup>, **1-trans** and **2-trans**.

<sup>a</sup> Institut für Chemie Humboldt-Universität zu Berlin, Brook-Taylor-Str. 2, 12489, Berlin, Germany. E-mail: kallol.ray@hu-berlin.de

<sup>b</sup> Anorganische Chemie 1 Ruhr-Universität Bochum, Universitätsstraße 150, 44780, Bochum, Germany

<sup>c</sup> Institut für Chemie Technische, Universität Berlin, Fakultät II Straße des 17. Juni 135, 10623, Berlin, Germany

<sup>d</sup> Institut für Physik Freie, Universität Berlin, Arnimallee 14, 14195 Berlin, Germany

<sup>e</sup> Department of Electrosynthesis, Fraunhofer UMSICHT, Osterfelder Str. 3, 46047 Oberhausen, Germany

† Electronic supplementary information (ESI) available. CCDC 2054129 and 2054130. For ESI and crystallographic data in CIF or other electronic format see DOI: 10.1039/d1cc00250c



containing a  $N_2S_2$  macrocyclic ligand, and  $[Fe^{IV}(O)(cyclam)(CH_3CN)]^{2+}$  (**2-trans**; cyclam = 1,4,8,11-tetraazacyclotetradecane; (Scheme 1)),<sup>26</sup> based on the popular  $N_4$ -donor cyclam ligand, provides some insight how *cis*-sulfur coordination influences the reactivity and spectroscopic properties of the oxoiron(IV) unit.

Combining the tetradentate dithiacyclam ligand with  $Fe(OTf)_2(CH_3CN)_2$  in acetonitrile yielded the iron(II) complex in two isomeric forms  $[Fe^{II}(\text{dithiacyclam})(CH_3CN)_2](OTf)_2$  (**1a-trans**) and  $[Fe^{II}(\text{dithiacyclam})(OTf)_2]$  (**1a-cis**). Crystals suitable for X-ray diffraction analysis were grown by vapour diffusion of diethyl ether into an acetonitrile solution of the iron(II) complex at  $-15^\circ\text{C}$  for **1a-cis** or at  $-40^\circ\text{C}$  for **1a-trans**. The X-ray structure of **1a-trans** displays a six-coordinate geometry with axially bound  $CH_3CN$  ligands (Fig. 1; Table S2, ESI<sup>†</sup>). The  $N_2S_2$  donor atoms of dithiacyclam occupy the equatorial coordination sites and show average Fe–S and Fe–N distances of 2.252(6) Å and 1.985(18) Å, respectively. In contrast, in **1a-cis** the sulfur donor atoms occupy the axial coordination sites and show average Fe–S distances of 2.466(14) Å (Table S1, ESI<sup>†</sup>); the nitrogen atoms of the dithiacyclam and the oxygen atoms of the triflate (OTf) anions occupy equatorial positions with average Fe–N and Fe–O distances of 2.2085(4) Å and 2.143(3) Å, respectively. The zero-field Mössbauer spectrum of **1a-cis** in acetone (Fig. S1, ESI<sup>†</sup>) at 15 K reveals a single quadrupole doublet with an isomer shift of  $\delta = 1.10\text{ mm s}^{-1}$  and a large quadrupole splitting of  $(\Delta E_Q) = 3.26\text{ mm s}^{-1}$ , demonstrating that the iron(II) center remains in the high-spin configuration ( $S = 2$ ). In addition, the  $^1\text{H}$ - and  $^{19}\text{F}$ -NMR spectra (Fig. S2, ESI<sup>†</sup>) of **1a-cis** in  $d_6$ -acetone at  $-85^\circ\text{C}$  display paramagnetically shifted peaks, indicative of the coordination of both OTf anions and further supporting the high-spin iron(II) assignment. In  $\text{CH}_2\text{Cl}_2/\text{CH}_3\text{CN}$  solution,  $\text{CH}_3\text{CN}$  gradually replaces the bound triflates of **1a-cis** to form **1a-trans** with an  $S = 0\text{ Fe}^{II}$  ground-state, as evident from  $^1\text{H}$ -NMR (at  $-85^\circ\text{C}$ ), which reveals peaks between 0 and 4 ppm (Fig. S3, ESI<sup>†</sup>, left), and  $^{19}\text{F}$ -NMR (at  $-85^\circ\text{C}$ ; Fig. S3, ESI<sup>†</sup>, right), which shows a singlet at  $-79.0\text{ ppm}$  corresponding to free OTf anions. Freezing the solution leads to the partial re-binding of OTf anion to  $\text{Fe}^{II}$ ; zero-field Mössbauer measurement (Fig. S4, ESI<sup>†</sup>) at 15 K shows a major quadrupole doublet with a new high-spin  $\text{Fe}^{II}$  signal ( $\delta = 1.15\text{ mm s}^{-1}$  and  $\Delta E_Q = 2.31\text{ mm s}^{-1}$ ; 73%) with a significantly reduced  $\Delta E_Q$  relative to **1a-cis**, presumably corresponding to the *trans*- $[(\text{dithiacyclam})\text{Fe}^{II}(\text{OTf})(\text{CH}_3\text{CN})]^+$  complex. An additional doublet with  $\delta = 0.52\text{ mm s}^{-1}$  and

$\Delta E_Q = 0.26\text{ mm s}^{-1}$  corresponds to the low-spin  $S = 0\text{ Fe}^{II}$  center in **1a-trans** (27%). Thus,  $\text{CH}_3\text{CN}$ -binding favours the *trans* configuration and the coordination of both  $\text{CH}_3\text{CN}$  is necessary for stabilizing the low-spin  $\text{Fe}^{II}$  state in **1a**.

A solution of **1a-trans** in a  $\text{CH}_2\text{Cl}_2/\text{CH}_3\text{CN}$  solvent mixture (95 : 5) at  $-85^\circ\text{C}$  with 4 equiv. of 2-(*tert*-butylsulfonyl)iodosylbenzene ( $t\text{BuSO}_2\text{C}_6\text{H}_4\text{IO}$ ,  $^s\text{PhIO}$ )<sup>27</sup> led to the formation of a pale green intermediate **1-trans** ( $t_{1/2} = 10\,000\text{ s}$  at  $-65^\circ\text{C}$ ) with absorption maxima at 596 nm ( $\epsilon_{\text{max}} = 226\text{ M}^{-1}\text{ cm}^{-1}$ ) and 815 nm ( $\epsilon_{\text{max}} = 549\text{ M}^{-1}\text{ cm}^{-1}$ ), which are typical of  $S = 1$  oxoiron(IV) cores (Fig. 2; left).<sup>11</sup> The characteristic near-infrared band in **1-trans** @ 815 nm is significantly red-shifted relative to that in **2-trans**,<sup>26</sup> which is consistent with a weakened equatorial field in **1-trans**. Notably, in the absence of  $\text{CH}_3\text{CN}$ , **1-trans** was not generated.<sup>28</sup> An electron spray ionization mass spectrum (Fig. S5, ESI<sup>†</sup>) of **1-trans** exhibited a signal at  $m/z = 794.96$ , consistent with its formulation as  $\{[(\text{dithiacyclam})\text{Fe}^{IV}(\text{O})(\text{OTf})](^s\text{PhIO})\}^+$  ( $m/z$  calc = 794.97), which is shifted by 4 units to  $m/z = 798.97$ , when  $\text{sPhI}^{18}\text{O}$  was used to generate **1-trans**.  $^{19}\text{F}$ -NMR (at  $-85^\circ\text{C}$  in a 95 : 5 mixture of  $\text{CD}_2\text{Cl}_2$  and  $\text{CD}_3\text{CN}$ ) shows a singlet at  $-77.0\text{ ppm}$  corresponding to the free OTf anions in **1-trans** (Fig. S6, ESI<sup>†</sup>). The zero-field Mössbauer spectrum of **1-trans** in frozen acetone/ $\text{CH}_2\text{Cl}_2/\text{CH}_3\text{CN}$  solution and recorded at 15 K exhibits a doublet representing about 84% of the iron with  $\Delta E_Q = 1.21\text{ mm s}^{-1}$  and  $\delta = 0.13\text{ mm s}^{-1}$  corresponding to the presence of an  $\text{Fe}^{IV}$  center (Fig. 2; right); the remaining 16% of the signals with  $\Delta E_Q = 1.57\text{ mm s}^{-1}$  and  $\delta = 0.55\text{ mm s}^{-1}$  correspond to a high-spin  $\text{Fe}^{III}$  product, arising from the decay of **1-trans**.

The Fe K-edge X-ray absorption (Fig. S7 and Table S4, ESI<sup>†</sup>) spectrum of **1-trans** reveals a K-edge energy of 7122.7 eV, which is lower relative to **2-trans** (7123.9 eV). Furthermore, the pre-edge transition in **1-trans** is less intense, which may reflect a less covalent  $\text{Fe}=\text{O}$  bond in **1-trans** relative to **2-trans**. The resonance Raman (rR) spectrum of **1-trans** exhibits a  $\nu(\text{Fe}=\text{O})$  stretching mode at  $793\text{ cm}^{-1}$  (Fig. 2, inset), which is red-shifted by  $49\text{ cm}^{-1}$  relative to that in **2-trans** ( $\nu(\text{Fe}=\text{O}) = 842\text{ cm}^{-1}$ ),<sup>26</sup> thereby demonstrating an elongation of the  $\text{Fe}=\text{O}$  bond by  $\sim 0.02\text{ Å}$  in **1-trans** relative to **2-trans**.<sup>29</sup> However, within the error of the



Fig. 1 Molecular structures of **1a-cis** and **1a-trans** obtained by XRD. Atoms are displayed as thermal ellipsoids at 50% probability level; triflate counter ions for **1a-trans** are omitted for clarity. Atom types: Fe: orange; N: blue; C: grey; O: red; S: yellow; F: green; H: white.



Fig. 2 Left: UV-Vis-spectrum of **1a-trans** (black) and **1-trans** (blue) in a 95 : 5 mixture of  $\text{CH}_2\text{Cl}_2$  and  $\text{CH}_3\text{CN}$  at  $-90^\circ\text{C}$ ; the inset shows the resonance Raman spectra of  $^{16}\text{O}$ - (black) and  $^{18}\text{O}$ -labelled (red) **1-trans** (4 mM) upon 413 nm irradiation at  $-90^\circ\text{C}$ . Solvent signal is indicated by an asterisk. Right: Zero-field Mössbauer spectrum (black) of a frozen sample of **1-trans** in a solvent mixture of acetone/ $\text{CH}_2\text{Cl}_2/\text{CH}_3\text{CN}$  (10 : 0.95 : 0.05) and simulation (red) with  $\delta = 0.13\text{ mm s}^{-1}$  and  $\Delta E_Q = 1.21\text{ mm s}^{-1}$  for the main species (blue, 84%). The minor species with  $\delta = 0.55\text{ mm s}^{-1}$  and  $\Delta E_Q = 1.57\text{ mm s}^{-1}$  corresponds to the decay of **1-trans** (brown, 16%).



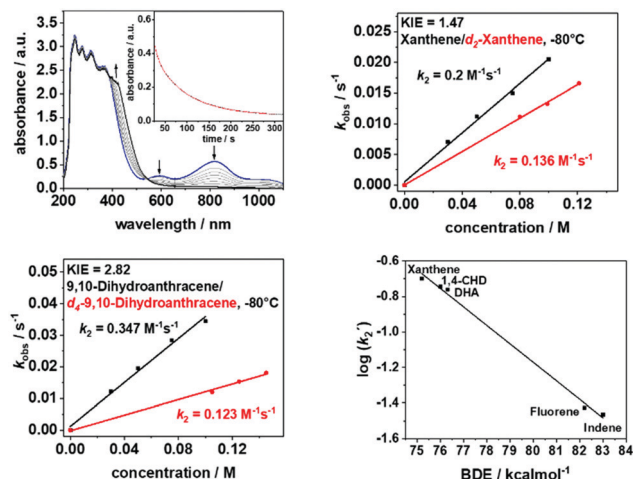


Fig. 3 Top left: Changes in the UV-Vis-spectra of a 1 mM solution of **1-trans** in  $\text{CH}_2\text{Cl}_2/\text{CH}_3\text{CN}$  (95:5) at  $-80^\circ\text{C}$  upon addition of 100 eq xanthene; the inset shows the time trace for the decay of the 815 nm band and its pseudo-first order fit; top right: plots of the pseudo-first order rate constants  $k_{\text{obs}}$  vs. the substrate concentrations for xanthene and  $d_2$ -xanthene in order to determine the kinetic isotopic effect (KIE) for the reaction of **1-trans** with xanthene; bottom left: plots of the pseudo-first order rate constants  $k_{\text{obs}}$  vs. the substrate concentrations for 9,10-dihydroanthracene (DHA) and  $d_4$ -DHA in order to determine the kinetic isotopic effect (KIE) for the reaction of **1-trans** with DHA; bottom right: plot of the logarithms of the second-order rate constants  $k_2'$  vs. the C-H BDEs of the substrates with **1-trans** in  $\text{CH}_2\text{Cl}_2/\text{CH}_3\text{CN}$  (95:5).

extended X-ray absorption fine structure (EXAFS) analysis, the Fe=O distances in **1-trans** and **2-trans** are not discernible; in both cases a distance of  $1.67 \pm 0.02 \text{ \AA}$  has been obtained.<sup>26</sup> The DFT optimized geometry of **1-trans** in the  $S = 1$  state slightly underestimates the Fe–O bond (calculated @  $1.655 \text{ \AA}$ ) from the EXAFS data (Tables S5 and S6, ESI†), and as a result the calculated  $\nu(\text{Fe–O})$  is overestimated. This is a common problem that is encountered in the oxoiron(IV) chemistry.<sup>8,13</sup> However, a geometry scan of the Fe–O bond length (Table S6, ESI†) reveals a relatively flat surface potential, with the structures exhibiting Fe–O bond lengths of  $1.66\text{--}1.70 \text{ \AA}$  being within  $1 \text{ kcal mol}^{-1}$  in energy from the lowest energy structure. In particular, a constrained optimization with a fixed Fe–O distance @  $1.68 \text{ \AA}$  for **1-trans** gives a calculated  $\nu(\text{Fe–O})$  of  $794 \text{ cm}^{-1}$ , in good agreement with the experiment. Similarly, a constrained geometry with an Fe–O distance of  $1.66 \text{ \AA}$  can account for the experimental  $\nu(\text{Fe–O})$  of

$842 \text{ cm}^{-1}$  for **2-trans**. In summary, a  $49 \text{ cm}^{-1}$  red-shift in the  $\nu(\text{Fe–O})$  of **1-trans** relative to **2-trans**, translates to an Fe=O elongation of only  $0.02 \text{ \AA}$  (based on both constrained DFT optimization and Badger's rule<sup>29</sup>), which is not clearly discernible within the error of the EXAFS analysis, but is reflected in a less-intense pre-edge transition at the Fe K-edge.

The introduction of the equatorial sulfur ligands also exhibits a significant effect on the reactivity of the oxoiron(IV) unit (Fig. 3 and Figs S8–S12, ESI†). In reactions with substrates containing C–H bonds like xanthene, 1,4-cyclohexadiene (CHD), dihydroanthracene (DHA), fluorene and indene, **1-trans** reacts at least 3–4 orders of magnitude faster than **2-trans** (Table 1). Furthermore, low kinetic isotope effects (KIEs) of 1.47 and 2.82 were determined in the reaction of **1-trans** with xanthene (Fig. 3, top right) and DHA (Fig. 3, bottom left), respectively, which are in contrast to the previously reported value of 20.0 for reaction of xanthene with **2-trans**.<sup>26</sup> Nevertheless, when the logarithms of the second order rate constants ( $k_2'$ ) were plotted vs. the BDE C–H values of the substrates, the linear correlation previously reported for **2-trans** were found to be also valid for **1-trans** (Fig. 3, bottom right). Thus, although proton-transfer is involved in the rate-determining step of the oxidation of C–H bonds by **1-trans**, the large tunneling contribution in hydrogen atom abstraction (HAA), which is observed in **2-trans** and in most high-valent metal-oxo mediated HAA reactions,<sup>11,12,30</sup> is not applicable for **1-trans**. In particular, in a previous study the axial thiolate ligand of  $[\text{Fe}^{\text{IV}}(\text{O})(\text{TMCS})]^+$  has been suggested to play a unique role in facilitating tunnelling, thereby resulting in a large KIE of 80 for DHA oxidation.<sup>31</sup> A contrasting effect is now demonstrated for the equatorial sulphur ligation, which reduces the tunnelling contribution to a minimum. The effect of N versus S donors in an otherwise identical ligand environment is also reflected in the higher oxygen atom transfer (OAT) ability of **1-trans** relative to **2-trans** (Table 1).

In summary, a minor  $0.02 \text{ \AA}$  elongation of the Fe=O bond upon introduction of the equatorial sulfur ligands is shown to have a dramatic influence on the spectroscopic (Table S7, ESI†) and oxidative reactivity properties of the  $\text{Fe}^{\text{IV}}=\text{O}$  unit. Notably, **1-trans**, similar to the previously reported<sup>13</sup>  $[(\text{Me}_3\text{TACN})\text{Fe}^{\text{IV}}(\text{O})(\text{S}_2\text{Si}(\text{CH}_3)_2)]$  complex features a very low  $\nu(\text{Fe–O})$ , which establishes a general trend of the activation of the Fe–O bond in oxoiron(IV) complexes involving *cis*-sulphur ligands. The enhanced reactivity of **1-trans** relative to **2-trans**, can presumably

Table 1 Reactivity comparison of **1-trans** and **2-trans**

Substrate	BDE <sup>a</sup> [kcal mol <sup>−1</sup> ]	$k_2$ [M <sup>−1</sup> s <sup>−1</sup> ] <b>1-trans</b>	$k_2$ [M <sup>−1</sup> s <sup>−1</sup> ] <b>2-trans</b>	Product (yield) <sup>d</sup>
Xanthene	75.2	205 <sup>b</sup>	$1.1 \times 10^{-1}$	Xanthone (36%)
1,4-CHD	76	370 <sup>b</sup>	$9.7 \times 10^{-2}$	
DHA	76.3	355 <sup>b</sup>	$4.9 \times 10^{-2}$	Anthracene (48%)
Fluorene	82.2	18.2 <sup>c</sup>	$7.1 \times 10^{-3}$	Fluorenone (11%)
Indene	83	17.6 <sup>c</sup>	$5.8 \times 10^{-3}$	Indenone
Thioanisole	—	87 <sup>c</sup>	—	
PPh <sub>3</sub>	—	n.d	5.9	OPPh <sub>3</sub> (28%)

<sup>a</sup> Values taken from ref. 32. <sup>b</sup> Values calculated for  $20^\circ\text{C}$  from experimental values determined at  $-80^\circ\text{C}$  using van't Hoff equation. <sup>c</sup> Values calculated for  $15^\circ\text{C}$  from experimental values determined at  $-65^\circ\text{C}$  using van't Hoff equation. <sup>d</sup> Specified yields correspond to the reactivity of **1-trans**. n.d: the reaction was too fast for kinetic studies.

be attributed to the positive shift in the redox potential upon sulphur ligation, as evident from cyclic voltammetry experiments, which shows a 170 mV positive shift in the  $\text{Fe}^{2+/3+}$  potential (Fig. S13, ESI†) in **1a-trans** relative to **2a-trans**. In addition, a change in mechanism in the C–H bond oxidation reactions from HAA to proton coupled electron transfer (PCET)<sup>33</sup> is evident from the reduction of KIE from a value of 20 in **2-trans** to 1.47 in **1-trans** (using xanthene as a substrate). This drastic downshift in KIE is unique for sulfur substitution and is not observed in the oxygen substituted oxoiron(IV) center.<sup>34</sup> Understanding this lowering of KIE will require further experimental and computational work. However the significant effect of the equatorial sulfur ligation on the physical and chemical properties of oxoiron(IV) cores may provide a compelling rationale for nature's use of the *cis*-thiolate ligated oxoiron(IV) motif in key metabolic transformations that involve the activation of strong C–H bonds.

This work was funded by the Deutsche Forschungsgemeinschaft (DFG, German Research Foundation) under Germany's Excellence Strategy – EXC 2008 – 390540038 – UniSysCat to K. R., P. H., and H. D., Excellence Strategy – EXC-2033 – Project number 390677874 to U.-P. A. and P. G., AP242/5-1 to U.-P. A. and the Heisenberg-Professorship and RA/2409/8-1 to K. R. We also thank the Fraunhofer Internal Programs under Grant No. Attract 097-602175 (U.-P. A.) and the Bundesministerium für Bildung und Forschung (BMBF, Operando-XAS project, 05K19KE1). The Helmholtz-Zentrum Berlin (HZB) is thanked for enabling the XAS experiments at KMC-3 of the BESSY synchrotron.

## Conflicts of interest

There are no conflicts to declare.

## Notes and references

- M. Costas, M. P. Mehn, M. P. Jensen and L. Que, *Chem. Rev.*, 2004, **104**, 939–986.
- B. Meunier, S. P. de Visser and S. Shaik, *Chem. Rev.*, 2004, **104**, 3947–3980.
- J. B. Gordon and D. P. Goldberg, *Reference Module in Chemistry, Molecular Sciences and Chemical Engineering*, Elsevier, 2020, DOI: 10.1016/B978-0-12-409547-2.14906-6.
- M. T. Green, J. H. Dawson and H. B. Gray, *Science*, 2004, **304**, 1653–1656.
- K. L. Stone, R. K. Behan and M. T. Green, *Proc. Natl. Acad. Sci. U. S. A.*, 2005, **102**, 16563–16565.
- J. Rittle and M. T. Green, *Science*, 2010, **330**, 933–937.
- F. Ogliaro, S. P. de Visser and S. Shaik, *J. Inorg. Biochem.*, 2002, **91**, 554–567.
- M. T. Green, *J. Am. Chem. Soc.*, 2006, **128**, 1902–1906.
- R. K. Behan, L. M. Hoffart, K. L. Stone, C. Krebs and M. T. Green, *J. Am. Chem. Soc.*, 2006, **128**, 11471–11474.
- K. L. Stone, R. K. Behan and M. T. Green, *Proc. Natl. Acad. Sci. U. S. A.*, 2006, **103**, 12307–12310.
- X. Engelmann, I. Monte-Pérez and K. Ray, *Angew. Chem., Int. Ed.*, 2016, **55**, 7632–7649.
- R. A. Baglia, J. P. T. Zaragoza and D. P. Goldberg, *Chem. Rev.*, 2017, **117**, 13320–13352.
- J. B. Gordon, A. C. Vilbert, I. M. DiMucci, S. N. MacMillan, K. M. Lancaster, P. Moënn-Loccoz and D. P. Goldberg, *J. Am. Chem. Soc.*, 2019, **141**, 17533–17547.
- L. Vicens, G. Olivo and M. Costas, *ACS Catal.*, 2020, **10**, 8611–8631.
- J. Chen, Z. Jiang, S. Fukuzumi, W. Nam and B. Wang, *Coord. Chem. Rev.*, 2020, **421**, 213443.
- T. Devi, Y.-M. Lee, W. Nam and S. Fukuzumi, *Coord. Chem. Rev.*, 2020, **410**, 213219.
- S. Fukuzumi, K.-B. Cho, Y.-M. Lee, S. Hong and W. Nam, *Chem. Soc. Rev.*, 2020, **49**, 8988–9027.
- S. Hong, Y.-M. Lee, K. Ray and W. Nam, *Coord. Chem. Rev.*, 2017, **334**, 25–42.
- W. Nam, Y.-M. Lee and S. Fukuzumi, *Acc. Chem. Res.*, 2018, **51**, 2014–2022.
- M. Sankaralingam, Y.-M. Lee, W. Nam and S. Fukuzumi, *Coord. Chem. Rev.*, 2018, **365**, 41–59.
- M. R. Bukowski, K. D. Koehntop, A. Stubna, E. L. Bominaar, J. A. Halfen, E. Münck, W. Nam and L. Que, *Science*, 2005, **310**, 1000–1002.
- D. Kumar, W. Thiel and S. P. de Visser, *J. Am. Chem. Soc.*, 2011, **133**, 3869–3882.
- S. Aluri and S. P. de Visser, *J. Am. Chem. Soc.*, 2007, **129**, 14846–14847.
- P. Gerschel, B. Battistella, D. Siegmund, K. Ray and U.-P. Apfel, *Organometallics*, 2020, **39**, 1497–1510.
- P. Gerschel, K. Warm, E. Farquhar, U. Englert, M. Reback, D. Siegmund, K. Ray and U.-P. Apfel, *Dalton Trans.*, 2019, **48**, 5923–5932.
- D. Kass, T. Corona, K. Warm, B. Braun-Cula, U. Kuhlmann, E. Bill, S. Mebs, M. Swart, H. Dau and M. Haumann, *J. Am. Chem. Soc.*, 2020, **142**, 5924–5928.
- D. Macikenas, E. Skrzypczak-Jankun and J. D. Protasiewicz, *J. Am. Chem. Soc.*, 1999, **121**, 7164–7165.
- Since we start with a pure solution of **1a-trans**, the sole product that is formed is **1-trans** (see also ref. 33). Oxidation of a solution of **1a-cis** leads to only iron(III) products; so we presume that **1-cis** is too unstable to be trapped in high-yields.
- According to Badger's rule (R. M. Badger, *J. Chem. Phys.*, 1935, **3**, 710–714), which is previously shown to be valid for oxoiron(IV) complexes (see ref. 8).
- (a) D. Mandal and S. Shaik, *J. Am. Chem. Soc.*, 2016, **138**, 2094–2097; (b) D. Mandal, D. Mallick and S. Shaik, *Acc. Chem. Res.*, 2018, **51**, 107–117; (c) E. J. Klinker, S. Shaik, H. Hirao and L. Que Jr., *Angew. Chem., Int. Ed.*, 2009, **48**, 1291–1295.
- J. E. M. N. Klein, D. Mandal, W.-M. Ching, D. Mallick, L. Que, Jr. and S. Shaik, *J. Am. Chem. Soc.*, 2017, **139**, 18705–18713.
- Y.-R. Luo, *Comprehensive Handbook of Chemical Bond Energies*, CRC Press, 2007, DOI: 10.1201/9781420007282.
- J. M. Meyer, *Acc. Chem. Res.*, 2010, **44**, 36–46.
- I. Monte-Pérez, X. Engelmann, Y.-M. Lee, M. Yoo, E. Kumaran, E. R. Farquhar, E. Bill, J. England, W. Nam, M. Swart and K. Ray, *Angew. Chem., Int. Ed.*, 2017, **56**, 14384–14388.

